◆ Human Brain Mapping 32:1973–1985 (2011) ◆

Correlation Between Gray Matter Density-Adjusted Brain Perfusion and Age Using Brain MR Images of 202 Healthy Children

Yasuyuki Taki,[1]* Hiroshi Hashizume,[1] Yuko Sassa,[1] Hikaru Takeuchi,[1] Kai Wu,[2] Michiko Asano,[1] Kohei Asano,[1] Hiroshi Fukuda,[2] and Ryuta Kawashima[1,3,4]

[1]*Division of Developmental Cognitive Neuroscience, Institute of Development, Aging and Cancer, Tohoku University, Senda, Japan*
[2]*Department of Nuclear Medicine & Radiology, Institute of Development, Aging and Cancer, Tohoku University, Sendai, Japan*
[3]*Department of Functional Brain Imaging, Institute of Development, Aging and Cancer, Tohoku University, Sendai, Japan*
[4]*Smart Ageing International Research Centre, Institute of Development, Aging and Cancer, Tohoku University, Sendai, Japan*

Abstract: We examined the correlation between brain perfusion and age using pulsed arterial spin-labeling (ASL) magnetic resonance images (MRI) in a large number of healthy children. We collected data on brain structural and ASL perfusion MRI in 202 healthy children aged 5–18 years. Structural MRI data were segmented and normalized, applying a voxel-based morphometric analysis. Perfusion MRI was normalized using the normalization parameter of the corresponding structural MRI. We calculated brain perfusion with an adjustment for gray matter density (BP-GMD) by dividing normalized ASL MRI by normalized gray matter segments in 22 regions. Next, we analyzed the correlation between BP-GMD and age in each region by estimating linear, quadratic, and cubic polynomial functions, using the Akaike information criterion. The correlation between BP-GMD and age showed an inverted U shape followed by a U-shaped trajectory in most regions. In addition, age at which BP-GMD was highest was different among the lobes and gray matter regions, and the BP-GMD association with age increased from the occipital to the frontal lobe via the temporal and parietal lobes. Our results indicate that higher order association cortices mature after the lower order cortices, and may help clarify the mechanisms of normal brain maturation from the viewpoint of brain perfusion. *Hum Brain Mapp 32:1973–1985, 2011.* © 2011 Wiley Periodicals, Inc.

Key words: arterial spin labeling; brain perfusion; children; gray matter; magnetic resonance imaging

Contract grant sponsor: Ministry of Education, Culture, Sports, Science and Technology Grant-in-Aid for Young Scientists; Contract grant number: 20790875.

*Correspondence to: Yasuyuki Taki, Division of Developmental Cognitive Neuroscience, Institute of Development, Aging & Cancer, Tohoku University, 4-1 Seiryocho, Aobaku, Sendai 980-8575, Japan. E-mail: ytaki@idac.tohoku.ac.jp

Received for publication 19 April 2010; Revised 8 July 2010; Accepted 17 August 2010

DOI: 10.1002/hbm.21163

Published online 21 January 2011 in Wiley Online Library (wileyonlinelibrary.com).

INTRODUCTION

Brain development continues through childhood and adolescence. Recently, it has been revealed that human brain development is a structurally and functionally nonlinear process [Giedd et al., 1999; Gogtay et al., 2004; Johnson, 2001; Lenroot et al., 2007; Thatcher, 1992]. For example, gray matter volume shows an inverted U-shaped curvilinear trajectory, with a pre-adolescent increase followed by a post-adolescent decrease in healthy children [Giedd et al., 1999; Gogtay et al., 2004; Lenroot et al., 2007]. This phenomenon is thought to derive from a corresponding increase and decrease in the number of synapses per neuron and intracortical myelination in brain maturation [Huttenlocher, 1979; Huttenlocher et al., 1982, 1997; Paus, 2005]. In addition, revealing the trajectory of brain perfusion in children is important because brain perfusion is thought to reflect cerebral metabolic demand [Chugani, 1998]. However, despite this growing wealth of knowledge about maturational changes in brain structure in children, the trajectory of brain perfusion with age in healthy children is not yet well documented.

Until recently, the measurement of brain perfusion has been performed by intravenous bolus injection of contrast agents or radioisotopes. Although these methods are important in acquiring quantitative measurements of brain perfusion, it is ethically problematic to apply these invasive methods to healthy children. More recently, arterial spin-labeling (ASL) perfusion magnetic resonance imaging (MRI) has been developed for evaluating brain perfusion [Williams et al., 1992]. In ASL, arterial blood water is magnetically labeled proximal to the tissue of interest, and the effects of this pre-labeling are determined by pair-wise comparison with images acquired using control labeling. This technique has been demonstrated to provide reproducible and reliable quantitative measurements of brain perfusion in various diseases and psychiatric disorders in adults [Alsop et al., 2000; Chalela et al., 2000; Chao et al., 2010; Detre et al., 1998; Du et al., 2006]. Because ASL is non-invasive and does not require intravenous injection of contrast agents or radioactive tracers, this method is appropriate for measuring brain perfusion of healthy children. In addition, because of the higher water content in children than in adults [Dobbing et al., 1973] and higher blood-flow velocities in carotid arteries in children than in adults [Schoning et al., 1993], the limitations of low signal-to-noise ratio and transit effects in ASL are actually reduced in children versus adults [Wang et al., 2006]. Using the ASL method, one study has shown a correlation between brain perfusion and age from 4 to 78 years [Biagi et al., 2007]. The study showed that perfusion in gray matter volume in the first decade of life was about two times higher than in the adult; brain perfusion then showed a decrease in adolescence, and finally reached the adult level, consistent with a study applying nuclear medicine methods such as ^{15}O-labeled positron emission tomography [Ye et al., 2000]. However, because that study showed a correlation between brain perfusion and age only in the global brain or in each lobe, the trajectory of brain perfusion of each gray matter region in healthy children has not yet been clarified. In addition, because of the limited spatial resolution of ASL as well as the findings of significantly higher brain perfusion in gray matter compared with white matter [Ito et al., 2005], observed brain perfusion derived from ASL images may produce partial volume biases, as is the case with brain perfusion images derived from nuclear medicine [Inoue et al., 2005; Matsuda et al., 2003; Meltzer et al., 1990; Muller-Gartner et al., 1992; Rousset et al., 1998; Strul et al., 1999; Videen et al., 1988]. Thus, the observed brain perfusion images potentially reflect amounts of gray matter as well as genuine brain perfusion. For these reasons, the observed brain perfusion should be adjusted by the amount of gray matter to obtain data on genuine brain perfusion. However, to date, no reported study has adjusted for the amount of gray matter in analyzing the correlation between brain perfusion and age in healthy children. Moreover, no reported study has examined the correlation between brain perfusion in each gray matter structure and age in a large number of healthy children. Because several disorders, such as autism, show significant differences in brain perfusion compared with age-matched normal children [Burroni et al., 2008; Gupta et al., 2009; Oner et al., 2005], evaluating the trajectory of brain perfusion with age in healthy children is thought to be important in understanding the mechanism(s) of brain maturation, as well as distinguishing normal brain maturation from pathology.

Thus, the purpose of the present study was to examine any correlation between brain perfusion, adjusted for gray matter density, and age in a large number of healthy children with a wide age range by applying region-of-interest (ROI) analysis, in which the gray matter region of the cerebrum was divided into four lobes and 22 ROIs, corresponding to anatomical structures in each hemisphere. Regarding the ASL, we used the Quantitative STAR labeling of Arterial Regions (QUASAR) implementation of pulsed ASL [Petersen et al., 2006a,b, 2010]. Using the QUASAR protocol, absolute brain perfusion can be quantified in well-characterized units of mL/100 g/min. Furthermore, the QUASAR protocol showed robust test–retest reliability in a multi-center study [Petersen et al., 2010]. We used gray matter density for the amount of gray matter, which was calculated by a voxel-based morphometric analysis [Good et al., 2001]. To examine any correlation between brain perfusion, with adjustment for gray matter density (BP-GMD), and age, the correlation was estimated using first-, second-, and third-order polynomial functions in each ROI. Then, we determined the best-fit model by selecting the function that showed the lowest Akaike information criterion (AIC) [Akaike, 1974]. We applied linear, quadratic, and cubic polynomial functions because we hypothesized that BP-GMD would show an inverted U shape followed by a U-shaped trajectory, as observed in cerebral metabolic rates of glucose utilization (CMRglu)

[Chugani, 1998] and number of synapses per neuron [Huttenlocher et al., 1997] in children. If this were the case, negative linear fitting could describe the portion between the peak of the inverted U-shaped and the U-shaped curve. Negative and positive quadratic fitting can describe the portion around the peak of the inverted U-shaped and the U-shaped trajectory, respectively. In addition, positive cubic fitting can describe the portion including the peaks of both trajectories. Moreover, by fitting the trajectory using polynomial functions, we can determine the age with the highest BP-GMD, which is thought to reflect progress in brain maturation. For example, the inverted U-shaped trajectory and the positive cubic trajectory directly show the age at which BP-GMD was highest. The negative linear and positive quadratic trajectories suggest that the age of highest BP-GMD is earlier than age range in this study. In addition, the regions fitted by a positive quadratic trajectory suggest earlier maturation than those fitted by a negative linear trajectory. Taken together, these data led us to hypothesize that the age of peak BP-GMD would be different among the lobes and gray matter regions and may show a progression from the occipital lobe to the frontal lobe via the temporal and parietal lobes, consistent with findings of brain structural maturation [Huttenlocher et al., 1997; Gogtay et al., 2004].

MATERIALS AND METHODS

Subjects

All subjects were healthy Japanese children who were recruited in the following manner. First, we distributed 29,740 advertisements summarizing this study to various kindergartens, elementary schools, junior high schools, and high schools in Miyagi Prefecture, Japan. Then, the 1,423 parents of subjects who had an interest in this study contacted us by mail. Next, we mailed both a child version and a parent version of the detailed information concerning the study to those parents. Then, 776 parents and subjects who were willing to participate contacted us again by mail. Subjects who had any history of malignant tumors, head traumas with a loss of consciousness lasting over 5 min, developmental disorders, epilepsy, psychiatric diseases, or claustrophobia were excluded by a preliminary telephone interview, a mail-in health questionnaire, and an oral interview. Of these subjects, we did not collect brain MR images from eight subjects due to claustrophobia (three subjects) and tiredness (five subjects). We collected brain MR images from 274 subjects in the order in which the notifications of their intention to participate in the project arrived by mail. No subjects were sedated during MR imaging. Trained examiners collected intelligence quotients (IQ) by administering the Japanese version of the Wechsler adult intelligence scale (WAIS), third edition [Fujita et al., 2006], to subjects whose ages were at least 16 years; for subjects aged less than 16 years, we used the Japanese version of the Wechsler intelligence scale for children (WISC), third edition [Azuma et al., 1998]. We calculated the full-scale IQ from the score of WAIS/WISC for each subject. Data from the MR images of 72 subjects were excluded because of motion artifacts, although ASL images of most of those subjects showed relatively slight motion artifacts. We excluded ASL image data with motion artifacts by visual inspection and by the voxel value (mL/100 g/min), which is indicative of actual brain perfusion. Specifically, if one or more voxels in the ASL image had a value higher than 150, we regarded the images as containing motion artifacts. Thus, the final sample consisted of 202 participants (95 boys, 107 girls). The ages of the subjects ranged from 5.7 to 18.4 years. The mean and SD of full-scale IQ of the subjects were 102.5 and 12.3, respectively. Age distribution of the subjects by gender is shown in Figure 1.

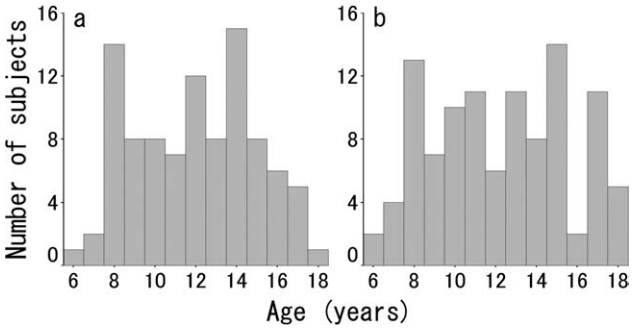

Figure 1.
Age distribution of male (**a**) and female (**b**) subjects.

Written informed consent was obtained from each subject and his/her parent after receipt of a full explanation of the purpose and procedures of the study, according to the Declaration of Helsinki [1991], prior to MR image scanning. Approval for these experiments was obtained from the institutional review board of Tohoku University.

Image Acquisition

All images were collected using a 3-T Philips Intera Achieva scanner. Three-dimensional, high-resolution, T1-weighted structural images were collected using a Magnetization Prepared Rapid Gradient Echo (MPRAGE) sequence. The parameters were as follows: 240 × 240 matrix, TR = 6.5 ms, TE = 3 ms, FOV = 24 cm, 162 slices, 1.0-mm slice thickness, scan duration 8 min 3 s. In addition, pulsed ASL brain perfusion images were collected in the state of eye closing by QUASAR implementation [Petersen et al., 2006a,b, 2010]. We determined the position of the slice by putting the fourth of the seven slices on the body of the corpus callosum in the coronal scout view. The parameters were as follows; 64 × 64 matrix, TR = 300 ms, TE = 22 ms, FOV = 24 cm, 7 slices, 7.0-mm slice thickness (2.0-mm gap), SENSE = 2.5, 84 averages, scan duration 5 min 52 s. Representative sets of ASL images in a

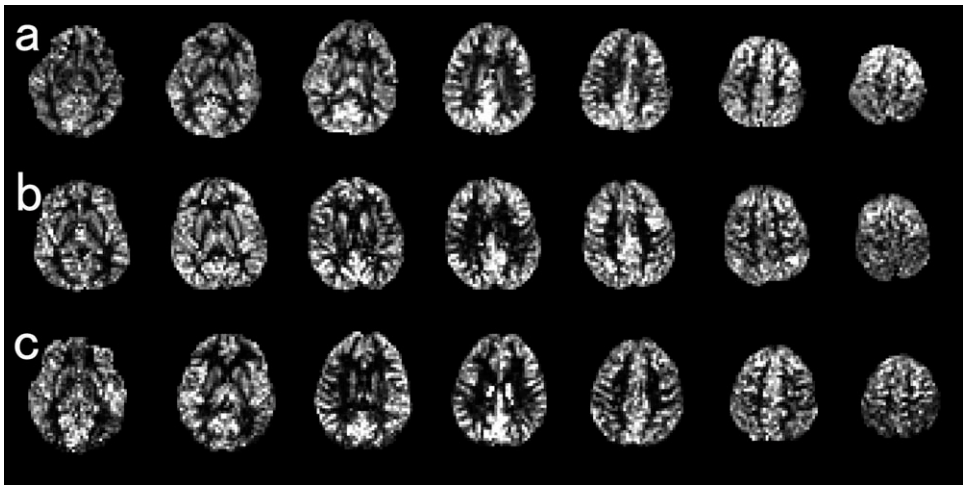

Figure 2.
Representative sets of ASL images in a 5.8-year-old female (**a**), a 9.6-year-old female (**b**), and a 13.5-year-old female (**c**).

5.8-year-old female, a 9.6-year-old female, and a 13.5-year-old female are shown in Figure 2.

Image Analysis of Structural MRI

A schematic of the image analysis is shown in Figure 3. After image acquisition by MRI, all T1-weighted MR images were analyzed using Statistical Parametric Mapping 2 (SPM2) (Wellcome Department of Cognitive Neurology, London, UK) [Friston et al., 1995] in Matlab (Math Works, Natick, MA) and part of the Matlab program "cg_vbm_optimized" (http://dbm.neuro.uni-jena.de/vbm. html). First, the T1-weighted MR images were transformed into Talairach stereotaxic space [Talairach and Tournoux, 1988] using a 12-parameter affine transformation [Ashburner et al., 1997] and the same template image. As the template image, we used the ICBM 152 template (Montreal Neurological Institute), which was derived from 152 normal subjects and which approximates Talairach space [Talairach and Tournoux, 1988]. Then, tissue segmentation from the transformed images to the gray matter, white matter, CSF space, and non-brain was performed using the SPM2 default segmentation procedure. Next, the segmented gray matter images were nonlinearly normalized to the gray matter template of SPM2, using $7 \times 8 \times 7$ nonlinear basis functions in three orthogonal directions. These normalization parameters were then reapplied to the T1-weighted whole brain structural images of each subject to perform optimal spatial normalization. The optimally normalized T1-weighted images were segmented into gray matter, white matter, and CSF space. Next, we set the ROI to frontal, occipital, parietal, and temporal lobes, and 22 additional ROIs that corresponded to gray matter structural regions of the cerebrum and of the deep gray matter structures in each hemisphere using "WFU_PickAtlas" [Lancaster et al., 2000; Maldjian et al., 2003] and obtained the regional gray matter density in each ROI bilaterally. The regional gray matter density in each ROI is shown in Table I for the left hemisphere and in Table II for the right hemisphere.

Image Analysis of Perfusion MRI

After image acquisition in ASL, all perfusion images were also analyzed using SPM2 [Friston et al., 1995] in Matlab. First, perfusion image voxel size was resized to match that of the MPRAGE images. Next, perfusion images were coregistered to corresponding gray matter segments in native space. Then, using the corresponding normalization parameter, derived from the normalization process of structural MR images, perfusion images were non-linearly normalized. Next, a gray matter binary mask image, consisting of a voxel value that was higher than an empirically determined value of 0.2 in the gray matter image, was applied to the perfusion images to reduce a partial volume effect of brain perfusion between gray matter and white matter. In addition, normalized gray matter segments were also masked using the corresponding gray matter masks. Next, we set the ROI to frontal, occipital, parietal, and temporal lobes and 22 ROIs by the same method as for the structural MRI described above, and obtained the regional brain perfusion in each ROI bilaterally. We acquired BP-GMD by dividing the average value of brain perfusion by average gray matter density in each ROI in each subject. The brain perfusion and BP-GMD for each ROI are shown in Table I for the left hemisphere and in Table II for the right hemisphere.

Statistical Analyses

To analyze the trajectory of BP-GMD with age, the correlation between BP-GMD and age was estimated using

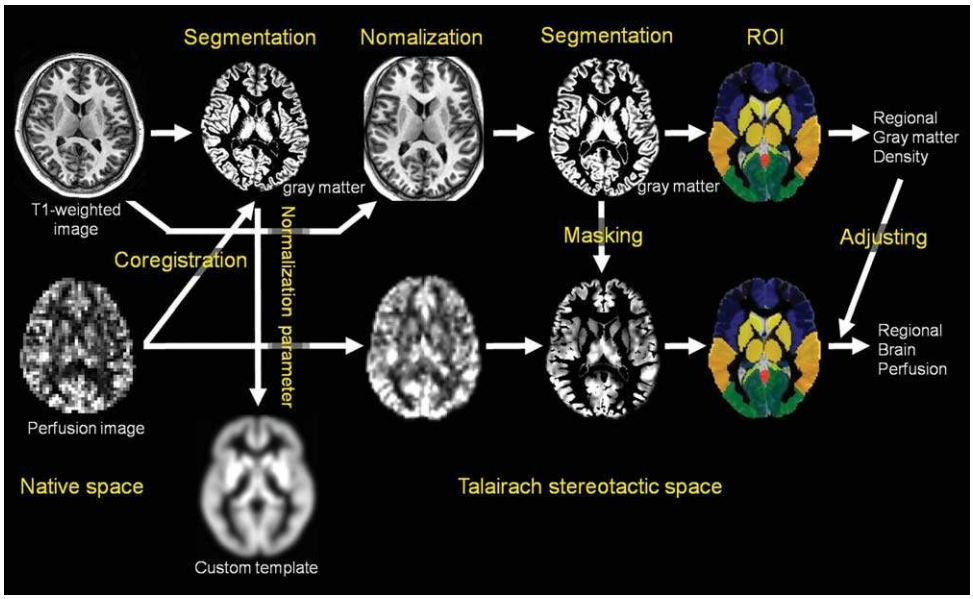

Figure 3.
Schematic of the image analysis.

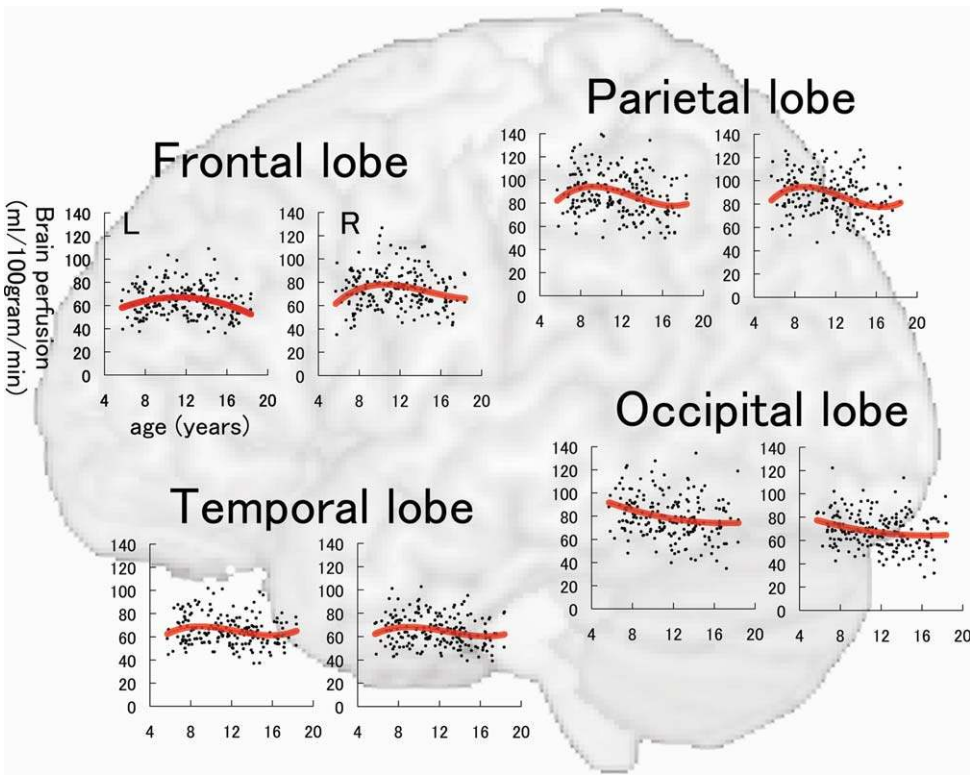

Figure 4.
Correlation between brain perfusion, adjusted for gray matter density, and age in the frontal lobe, parietal lobe, occipital lobe, and temporal lobe in each hemisphere. In each graph, the correlation was fitted by linear, quadratic, or cubic polynomial functions, determined by the Akaike Information Criterion. In each graph, the vertical axis indicates partial volume-correction-adjusted brain perfusion (unit, mL/100 g/min), and the horizontal axis refers to age (unit, years).

TABLE I. Mean and standard deviation of regional gray matter volume, regional perfusion, and gray matter volume-adjusted brain perfusion in each ROI in the left hemisphere

Structure	Gray matter[a]	Perfusion[b]	BP-GMD[c]	Trajectory[d]	Adjusted R^2	P age[ne]
Frontal lobe	0.481 (0.031)	39.14 (7.86)	64.06 (13.28)	Quadratic, negative	0.047	0.001
Parietal lobe	0.463 (0.036)	40.27 (8.02)	87.52 (18.92)	Cubic, positive	0.072	0.094
Occipital lobe	0.613 (0.032)	36.68 (8.54)	79.46 (18.53)	Quadratic, positive	0.059	0.281
Temporal lobe	0.610 (0.034)	39.75 (7.54)	65.34 (12.43)	Cubic, positive	0.032	0.081
Angular gyrus	0.549 (0.068)	41.42 (10.41)	76.20 (20.04)	Cubic, positive	0.079	0.164
Anterior cingulate cortex	0.586 (0.046)	41.01 (8.56)	70.39 (15.32)	Cubic, positive	0.013	0.189
Caudate nucleus	0.774 (0.042)	29.20 (6.74)	37.79 (8.72)	Cubic, positive	0.019	0.172
Cingulate gyrus	0.499 (0.046)	42.82 (8.48)	86.56 (19.31)	Cubic, positive	0.014	0.303
Cuneus	0.575 (0.032)	39.03 (9.43)	67.59 (16.42)	Quadratic, positive	0.039	0.216
Hippocampus	0.758 (0.030)	31.20 (7.13)	41.28 (9.79)	Cubic, positive	0.016	0.233
Inferior frontal gyrus	0.565 (0.028)	39.56 (8.36)	70.31 (15.59)	Quadratic, negative	0.053	0.004
Inferior parietal lobule	0.469 (0.041)	40.97 (8.11)	88.24 (19.81)	Cubic, positive	0.075	0.071
Insula	0.615 (0.039)	39.17 (7.31)	64.03 (13.11)	Quadratic, negative	0.024	0.114
Medial superior frontal gyrus	0.487 (0.034)	39.96 (8.26)	82.39 (17.58)	Quadratic, negative	0.027	0.007
Middle frontal gyrus	0.490 (0.032)	41.02 (9.05)	84.08 (19.62)	Quadratic, negative	0.069	<0.001
Middle temporal gyrus	0.635(0.039)	35.85 (8.61)	56.46 (13.16)	Cubic, positive	0.108	0.037
Paracentral lobule	0.486 (0.032)	38.05 (8.91)	78.71 (19.71)	Quadratic, negative	0.039	0.093
Posterior cingulate cortex	0.689 (0.038)	47.62 (10.58)	69.13 (15.28)	Linear, negative	0.087	<0.001
Postcentral gyrus	0.445 (0.030)	33.80 (7.28)	76.43 (17.88)	Cubic, positive	0.048	0.175
Precentral gyrus	0.476 (0.027)	34.76 (7.31)	73.34 (16.16)	Cubic, positive	0.064	0.185
Precuneus	0.523 (0.040)	45.70 (10.12)	87.82 (20.36)	Cubic, positive	0.091	0.165
Superior frontal gyrus	0.457 (0.028)	40.30 (9.20)	88.39 (20.17)	Quadratic, negative	0.091	<0.001
Superior occipital gyrus	0.623 (0.049)	30.36 (11.84)	48.93 (19.25)	Linear, negative	0.072	<0.001
Superior temporal gyrus	0.601 (0.027)	42.82 (8.09)	71.21 (13.83)	Cubic, positive	0.047	0.092
Supramarginal gyrus	0.497 (0.062)	40.48 (8.80)	82.59 (20.56)	Cubic, positive	0.040	0.169
Thalamus	0.743 (0.034)	35.71 (7.68)	48.18 (10.63)	Cubic, positive	0.024	0.041

[a]Regional gray matter density, mean (SD).
[b]Regional perfusion, mean (SD). Unit is mL/100 g/min.
[c]Brain perfusion with adjustment of the gray matter density, mean (SD).
[d]Best fit model of the correlation between age and gray matter volume-adjusted brain perfusion determined by the Akaike Information Criterion.
[e]The P value for the unique contribution of age in a linear model, age^2 in a quadratic model, or age^3 in a cubic model to the explained variance in gray matter volume-adjusted brain perfusion.

linear, quadratic, and cubic polynomial functions in global gray matter and in each ROI. We determined the best-fit model by selecting the function that showed the smallest AIC [Akaike, 1974]. By AIC, information regarding the best-fit model can be obtained, which was our primary purpose, whereas information regarding statistical significance is not obtained. However, as a reference, we described the adjusted R^2 in each fitting as well as the P value for the unique contribution of age in a linear model, age^2 in a quadratic model, or age^3 in a cubic model to the explained variance in BP-GMD in Tables I and II.

RESULTS

The Correlation Between Age and BP-GMD in Each Lobe

The results of model fitting for the correlation between BP-GMD and age are shown in Table I for the left hemisphere and Table II for the right hemisphere. The correlation between age and BP-GMD in each lobe is shown in Figure 4. In the frontal lobe, both hemispheres showed inverted U-shaped trajectories for the correlation between BP-GMD and age. The left hemisphere was best fitted by a negative quadratic polynomial function [adjusted R^2, 0.047; P age^2 (P value for the unique contribution of the age^2), 0.001], and the right hemisphere by the positive cubic polynomial function (adjusted R^2, 0.042; P age^3, 0.227). The estimated age for the highest BP-GMD in the left hemisphere was 11.3 years old and for the right hemisphere, 10.5 years old. In the parietal lobe, both hemispheres showed an inverted U shape followed by a U-shaped curve trajectory for the correlation between BP-GMD and age. In both hemispheres, the best fit was by a positive cubic polynomial function (left; adjusted R^2, 0.072; P age^3, 0.094; right; adjusted R^2, 0.091; P age^3, 0.043). The estimated age at which BP-GMD was highest in the left hemisphere was 9.2 years old and in the right hemisphere, 8.9 years old. In the temporal lobe, both hemispheres

TABLE II. Mean and standard deviation of regional gray matter volume, regional perfusion, and gray matter volume-adjusted brain perfusion in each ROI in the right hemisphere

Structure	Gray matter[a]	Perfusion[b]	BP-GMD[c]	Trajectory[d]	Adjusted R^2	P age[ne]
Frontal lobe	0.492 (0.030)	36.13 (7.27)	73.73 (15.82)	Cubic, positive	0.042	0.227
Parietal lobe	0.481 (0.035)	41.75 (8.37)	87.31 (18.73)	Cubic, positive	0.091	0.043
Occipital lobe	0.604 (0.031)	41.12 (9.16)	68.04 (14.81)	Quadratic, positive	0.049	0.260
Temporal lobe	0.629 (0.032)	40.65 (7.91)	64.77 (12.78)	Cubic, positive	0.032	0.170
Angular gyrus	0.587 (0.059)	40.63 (10.04)	69.57 (17.24)	Cubic, positive	0.105	0.018
Anterior cingulate cortex	0.587 (0.045)	38.85 (8.34)	66.66 (15.61)	Cubic, positive	0.016	0.170
Caudate nucleus	0.793 (0.038)	26.95 (6.24)	34.00 (7.89)	Cubic, positive	0.002	0.301
Cingulate gyrus	0.502 (0.045)	45.46 (8.96)	91.52 (20.89)	Cubic, positive	0.013	0.310
Cuneus	0.567 (0.029)	42.57 (10.16)	75.08 (17.84)	Linear, negative	0.036	0.004
Hippocampus	0.732 (0.033)	33.74 (7.54)	46.15 (10.51)	Quadratic, positive	0.013	0.057
Inferior frontal gyrus	0.567 (0.029)	35.08 (7.62)	62.08 (14.23)	Quadratic, negative	0.036	0.012
Inferior parietal lobule	0.506 (0.042)	41.33 (8.63)	82.19 (18.54)	Cubic, positive	0.074	0.035
Insula	0.648 (0.034)	37.48 (7.38)	58.07 (12.11)	Linear, positive	0.012	0.065
Medial superior frontal gyrus	0.495 (0.035)	39.16 (8.11)	79.50 (17.54)	Cubic, positive	0.038	0.143
Middle frontal gyrus	0.505 (0.031)	36.78 (8.17)	73.28 (17.51)	Cubic, positive	0.039	0.246
Middle temporal gyrus	0.662 (0.035)	38.03 (8.78)	57.52 (13.32)	Linear, negative	0.090	<0.001
Paracentral lobule	0.463 (0.027)	41.16 (8.83)	89.49 (20.93)	Quadratic, negative	0.031	0.087
Posterior cingulate cortex	0.697 (0.033)	52.40 (12.05)	75.33 (17.66)	Linear, negative	0.115	<0.001
Postcentral gyrus	0.456 (0.030)	34.36 (7.32)	75.84 (17.50)	Cubic, positive	0.069	0.109
Precentral gyrus	0.490 (0.025)	32.74 (7.13)	67.05 (15.17)	Cubic, positive	0.064	0.237
Precuneus	0.514 (0.037)	49.31 (10.93)	96.38 (22.11)	Linear, negative	0.103	0.167
Superior frontal gyrus	0.468 (0.029)	37.01 (8.21)	79.36 (18.02)	Cubic, positive	0.071	0.170
Superior occipital gyrus	0.615 (0.043)	32.96 (12.57)	53.84 (20.77)	Linear, negative	0.066	0.001
Superior temporal gyrus	0.630 (0.026)	42.51 (8.46)	67.61 (13.65)	Cubic, positive	0.059	0.180
Supramarginal gyrus	0.550 (0.060)	44.19 (9.79)	81.06 (19.47)	Cubic, positive	0.047	0.059
Thalamus	0.797 (0.032)	36.13 (7.54)	45.37 (9.48)	Cubic, positive	0.033	0.063

[a]Regional gray matter density, mean (SD).
[b]Regional perfusion, mean (SD). Unit is mL/100 g/min.
[c]Brain perfusion with adjustment of the gray matter density, mean (SD).
[d]Best fit model of the correlation between age and gray matter volume-adjusted brain perfusion, determined by the Akaike Information Criterion.
[e]The P value for the unique contribution of age in a linear model, age^2 in a quadratic model, or age^3 in a cubic model to the explained variance in gray matter volume-adjusted brain perfusion.

showed an inverted U shape followed by a U-shaped curve trajectory for the correlation between BP-GMD and age. In both hemispheres, the best fit was by a positive cubic polynomial function (left; adjusted R^2, 0.032; P age^3, 0.081; right; adjusted R^2, 0.032; P age^3, 0.170). The estimated age at which BP-GMD was highest in the left hemisphere was 9.4 years old and in the right hemisphere, 9.0 years old. In the occipital lobe, both hemispheres showed a U-shaped trajectory for the correlation between BP-GMD and age. In both hemispheres, the best fit was by a positive quadratic polynomial function (left; adjusted R^2, 0.059; P age^2, 0.281; right; adjusted R^2, 0.049; P age^2, 0.260). Estimated age in the highest BP-GMD in left hemisphere is thought to be younger than our age range in this study.

Correlation Between Age and BP-GMD in Each ROI

The results of model fitting for the correlation between BP-GMD and age are shown in Table I for the left hemisphere and Table II for the right hemisphere. The correlation between age and BP-GMD in each gray matter region is shown in Figure 5 for the lateral frontal and temporal lobes, Figure 6 for the lateral parietal and occipital lobes, Figure 7 for the medial aspect of the cerebrum, and Figure 8 for deep gray matter regions. In the frontal lobe, all gray matter regions showed an inverted U-shaped trajectory for the correlation between BP-GMD and age, and the best fit was a negative quadratic or positive cubic polynomial function. The estimated age at which BP-GMD was highest was earlier in the precentral gyrus, cingulate gyrus, and anterior cingulate cortex than in the superior, middle, and inferior frontal gyri. In the parietal lobe, gray matter regions of the lateral sides, such as the postcentral gyrus, supramarginal gyrus, angular gyrus, and inferior parietal lobule, showed inverted U-shaped trajectories in the correlation between BP-GMD and age, and the best fit was a positive cubic polynomial function. On the other hand, gray matter regions of the medial side, such as the precuneus and posterior cingulate cortex, were best fit by

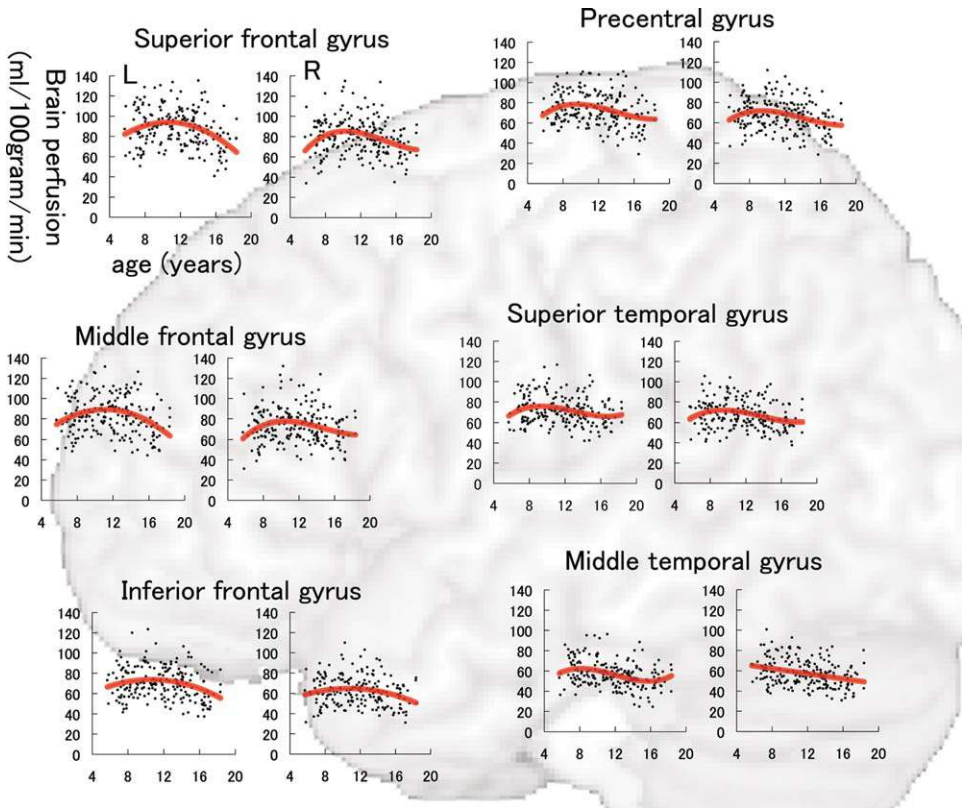

Figure 5.

Correlation between brain perfusion, adjusted for gray matter density, and age in the precentral gyrus, superior frontal gyrus, middle frontal gyrus, inferior frontal gyrus, superior temporal gyrus, and middle temporal gyrus. Details are the same as those in Figure 4.

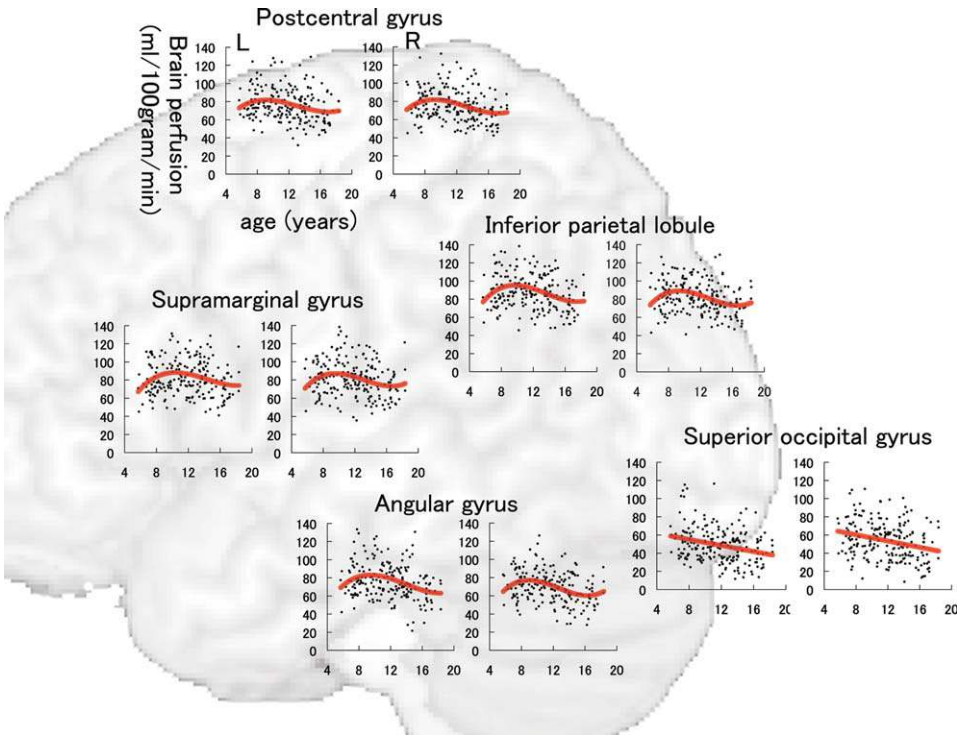

Figure 6.

Correlation between brain perfusion, adjusted for gray matter density, and age in the postcentral gyrus, supramarginal gyrus, angular gyrus, inferior parietal lobule, and superior occipital gyrus. Details are the same as those in Figure 4.

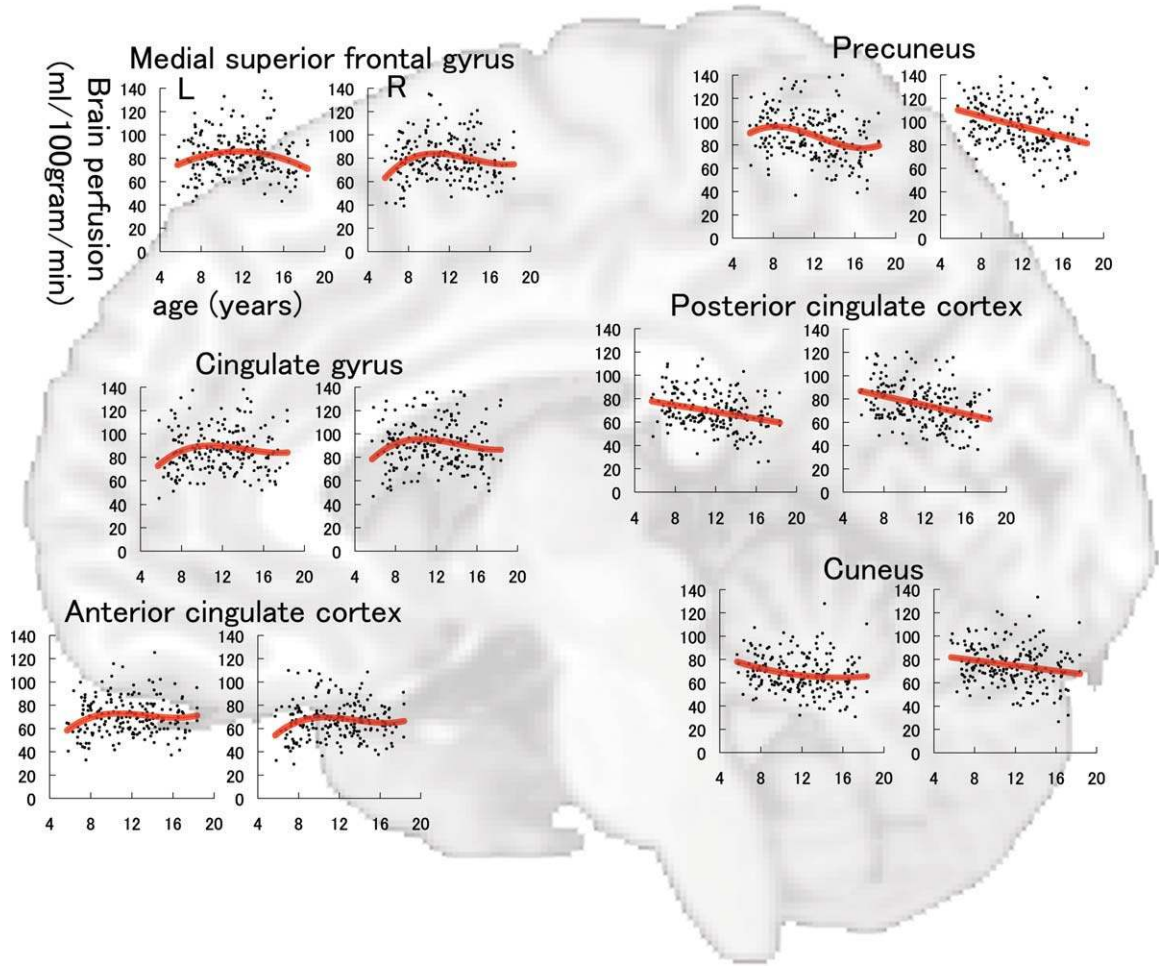

Figure 7.

Correlation between brain perfusion, adjusted for gray matter density, and age in the medial aspect of the superior frontal gyrus, cingulate gyrus, anterior cingulate cortex, posterior cingulate cortex, precuneus, and cuneus. Details are the same as those in Figure 4.

negative linear regression, except for the left precuneus. The estimated age at which BP-GMD was highest was earlier in the medial side than the lateral side of the parietal lobe. In the temporal lobe, gray matter regions of the lateral side, such as the superior and middle temporal gyri, showed inverted U-shaped trajectories for the correlation between BP-GMD and age, and the best fit was a positive cubic polynomial function. Although the gray matter region of the hippocampus was also best fit by a positive cubic polynomial function, the trajectory of the correlation was rather flat or U-shaped. In the occipital lobe, gray matter regions of the superior occipital gyrus and the cuneus showed U-shaped trajectories or a negative linear correlation between BP-GMD and age, and the best fit was a linear or quadratic polynomial function. The estimated age at which BP-GMD was highest is thought to be younger than the age range in this study.

DISCUSSION

To the best of our knowledge, this is the first report of a correlation between BP-GMD and age, applying ASL perfusion MRI over a wide age range of healthy children. In particular, this study provided two novel findings. First, as hypothesized, the trajectory of BP-GMD showed an inverted U shape followed by a U-shaped curvilinear pattern in most brain regions, similar to the trajectories derived from brain structural and functional studies regarding brain maturation [Chugani, 1998; Gogtay et al., 2004; Huttenlocher et al., 1997]. Second, as hypothesized, the age at which BP-GMD was highest was different among the lobes and gray matter regions and progressed from the occipital lobe to the frontal lobe via the temporal and parietal lobes.

We demonstrated that BP-GMD in most ROIs showed an inverted U-shape followed by a U-shaped curvilinear

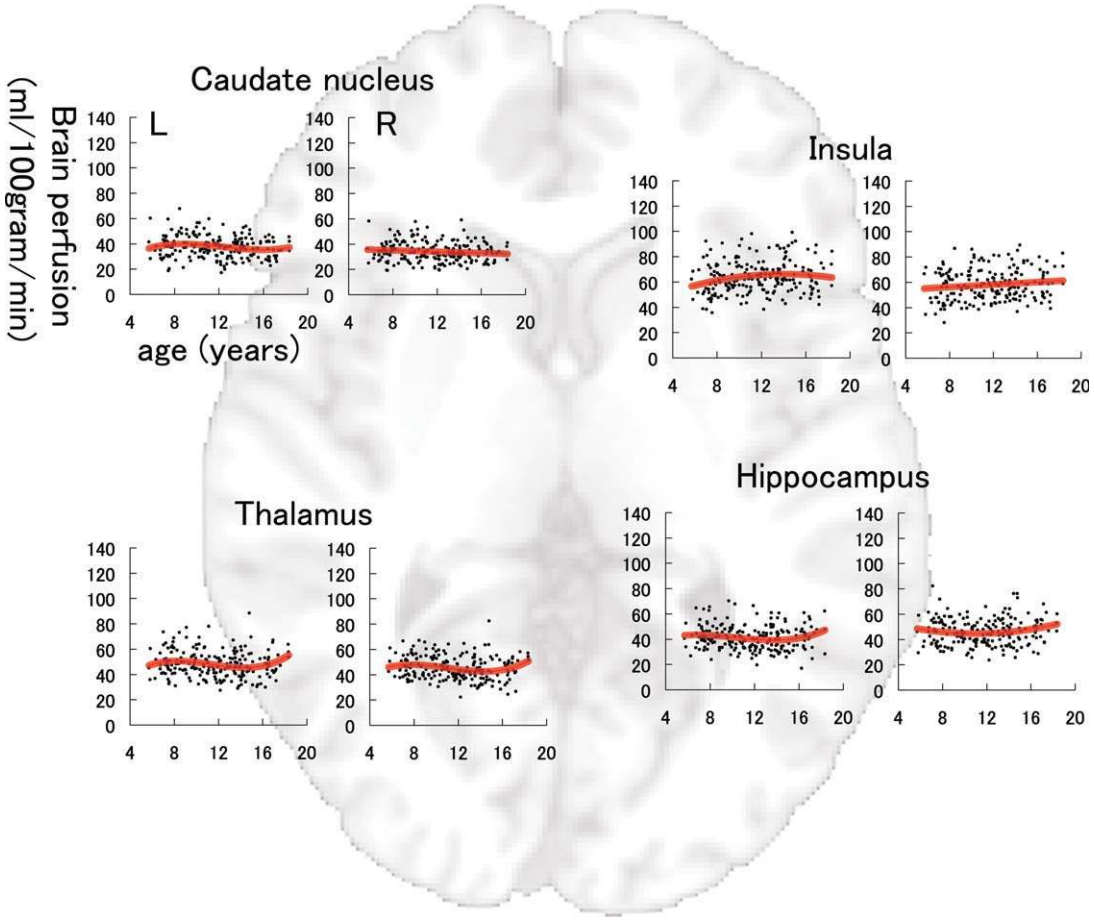

Figure 8.
Correlation between brain perfusion, adjusted for gray matter density, and age in the caudate nucleus, thalamus, insula, and hippocampus. Details are the same as those in Figure 4.

trajectory in children. These results are partially consistent with a recent study that showed a correlation between brain perfusion and age across a wide age range [Biagi et al., 2007]. The shape of the trajectory was similar between that study and our results, although the brain perfusion values were slightly higher in this study than the previous study. The difference is thought to be due to the methodologies used. We adjusted gray matter density in estimating brain perfusion to remove the effect of the amount of gray matter, whereas the previous study did not. Regarding the mechanism of the curvilinear trajectory, recent studies have shown that a pre-adolescent increase followed by a post-adolescent decrease in the number of synapses per neuron and intracortical myelination occur during brain maturation [Huttenlocher, 1979; Huttenlocher et al., 1982, 1997; Paus, 2005]. Because a major portion of the glucose consumed by the brain is used for the maintenance of resting membrane potentials [Mata et al., 1980], there should be a direct relationship between the degree of synaptic connectivity, or dendritic arborization, and the CMRglu. In fact, the trajectory of the CMRglu in the first and second decade of life shows an increase twice as great as that seen in adults during the first 4–10 years, then it shows a gradual decline until adult CMRglu values are reached around the age of 16–18 years [Chugani, 1998]. Because of the relationship between CBF and glucose consumption [Fox et al., 1986, 1988; Newberg et al., 2005], an inverted U shape followed by a U-shaped curvilinear trajectory of BP-GMD is observed in healthy children.

We showed that the age at which BP-GMD was highest moved in a posterior to anterior direction. In detail, the peak age of BP-GMD in the occipital lobe was estimated at less than 5 years, those in temporal and parietal lobes were about 9 years, and that of the frontal lobe was about 11 years. Recent post-mortem studies of human brains showed that the time course of synaptogenesis was earlier in the visual cortex and auditory cortex than in the prefrontal cortex [Huttenlocher, 1979; Huttenlocher et al., 1982, 1997]. In addition, synapse elimination starts earlier

in the visual cortex than in the auditory cortex, and that in the prefrontal cortex starts later than in both former regions [Huttenlocher et al., 1997]. These results suggest that brain maturation starts in the occipital lobe, and then moves to the temporal lobe, followed by the frontal lobe. From those studies and our results, the trajectory of brain maturation from the viewpoint of synaptogenesis and synapse elimination, as well as BP-GMD, progresses from the occipital lobe to the frontal lobe. These phenomena support the idea that cortical development follows the evolutionary sequence to some degree [Gogtay et al., 2004]. Interestingly, the timing of synapse elimination progresses earlier than the decrease in brain perfusion. One reasons for this difference is thought to be intracortical myelination [Paus, 2005], which also progresses in the caudal-to-rostral direction [Webb et al., 2001] and is thought to occur in parallel with synapse elimination [Gogtay et al., 2004]. Because of metabolic demand for myelination, brain perfusion is thought to maintain high values at the time synapse elimination begins.

We also demonstrated that the peak age of BP-GMD was different within each lobe. In the frontal lobe, the peak age of BP-GMD of the precentral gyrus was about 8–10 years, whereas that of the superior, middle, and inferior frontal gyri was around 12 years. In addition, the peak age of BP-GMD of the precuneus and the posterior cingulate cortex was around 8 years or earlier, whereas that of the lateral parietal regions, such as the supramarginal gyrus and angular gyrus, was around 10 years. These findings are consistent with a recent study that showed a correlation between regional gray matter volume and age in healthy children [Gogtay et al., 2004]. That study showed that structural maturation progressed from the back to the front in the frontal lobe, and from the front to the lateral regions in the parietal lobe. The results of that study and our results may indicate that brain regions involved in basic functions, such as motor and sensory functions, mature first, followed by the regions involved in higher cognitive function, such as executive function [Ardila, 2008]. On the other hand, the hippocampus and deep gray matter regions, such as the caudate nucleus and the thalamus, showed relatively subtle change in brain perfusion compared with other regions. A recent study showed a correlation between age and gray matter volume in subcortical brain structures such as the caudate head, thalamus, and hippocampus [Ostby et al., 2009]. That study revealed that most subcortical regions showed a weaker relationship between age and gray matter volume compared with the cortex [Ostby et al., 2009]. Thus, it is thought that the relatively minor changes in BP-GMD are related to relatively slight changes in gray matter volume in several subcortical brain structures in children, because the metabolic demand of gray matter is thought to be positively correlated with the extent of gray matter volume change due to maturation. In addition, we showed that a slight increase in BP-GMD was observed in the hippocampus. This may be related to the result that hippocampal volume increases in adolescence and young adulthood [Guo et al., 2007; Ostby et al., 2009].

This study has several limitations. First, we did not acquire the data for brain perfusion in the ventral and dorsal aspects due to limitations in QUASAR range. If we performed a continuing two-time acquisition of QUASAR data, we could cover the whole brain in terms of brain perfusion. In fact, we did do this for 10 subjects, but because the acquisition time doubled, many more motion artifacts were observed, and we could not use any of the data. Thus, to minimize the acquisition time, we did not acquire the data on brain perfusion in the ventral and dorsal aspects. Second, this was a cross-sectional study; that is, we have shown a relationship between brain perfusion and age, but we have not shown a relationship over time. Thus, we are planning to perform a longitudinal analysis to examine the correlation between brain perfusion and age. Third, we did not analyze the effect of gender or hemisphere on maturational trajectory of BP-GMD because neither was a primary focus. However, to adjust the structural differences derived from differences in gender and hemisphere, we used BP-GMD instead of apparent brain perfusion.

In conclusion, we demonstrated a correlation between BP-GMD and age using ASL brain perfusion MRI in a large number of healthy children over a wide age range. As a result, the trajectory of the correlation between BP-GMD and age showed an inverted U-shaped second-order polynomial function in most regions in the frontal lobe, a third-order polynomial function in the parietal and temporal lobes, and a U-shaped second-order and negative linear correlation in the occipital lobe. Our results indicate that higher order association cortices mature after the lower order cortices in terms of brain perfusion. As a result, the trajectory of the correlation between BP-GMD and age showed an inverted U shape followed by a U-shaped trajectory in most regions. In addition, the age at which BP-GMD was highest was different among the lobes and gray matter regions, showing a progression from the occipital lobe to the frontal lobe, via the temporal and parietal lobes. Our results indicate that higher order association cortices mature after the lower order cortices mature. This may help not only clarify the mechanisms of normal brain maturation from the viewpoint of brain perfusion, but also distinguish normal from developmental disorders that show abnormal brain perfusion patterns.

ACKNOWLEDGMENTS

The authors thank R. Goto, K. Sato, and S. Kinomura for image analysis, Y. Yamada, Y. Kotozaki, and R. Nouchi for collecting MR data, and Y. Suzuki for technical support.

REFERENCES

Akaike H (1974): A new look at statistical model identification. IEEE Trans Automatic Control 19:716–723.

Alsop DC, Detre JA, Grossman M (2000): Assessment of cerebral blood flow in Alzheimer's disease by spin-labeled magnetic resonance imaging. Ann Neurol 47:93–100.

Ardila A (2008): On the evolutionary origins of executive functions. Brain Cogn 68:92–99.

Ashburner J, Neelin P, Collins DL, Evans A, Friston K (1997): Incorporating prior knowledge into image registration. Neuroimage 6:344–352.

Azuma H, Ueno K, Fujita K, Maekawa H, Ishikuma T, Sano H (1998): Japanese Wechsler Intelligence Scale for Children, 3rd ed. Tokyo: Nihon Bunka Kagakusha.

Biagi L, Abbruzzese A, Bianchi MC, Alsop DC, Del Guerra A, Tosetti M (2007): Age dependence of cerebral perfusion assessed by magnetic resonance continuous arterial spin labeling. J Magn Reson Imaging 25:696–702.

Burroni L, Orsi A, Monti L, Hayek Y, Rocchi R, Vattimo AG (2008): Regional cerebral blood flow in childhood autism: A SPET study with SPM evaluation. Nucl Med Commun 29:150–156.

Chalela JA, Alsop DC, Gonzalez-Atavales JB, Maldjian JA, Kasner SE, Detre JA (2000): Magnetic resonance perfusion imaging in acute ischemic stroke using continuous arterial spin labeling. Stroke 31:680–687.

Chao LL, Buckley ST, Kornak J, Schuff N, Madison C, Yaffe K, Miller BL, Kramer JH, Weiner MW (2010): ASL perfusion MRI predicts cognitive decline and conversion from MCI to dementia. Alzheimer Dis Assoc Disord 24:19–27.

Chugani HT (1998): A critical period of brain development: Studies of cerebral glucose utilization with PET. Prev Med 27:184–188.

Detre JA, Alsop DC, Vives LR, Maccotta L, Teener JW, Raps EC (1998): Noninvasive MRI evaluation of cerebral blood flow in cerebrovascular disease. Neurology 50:633–641.

Dobbing J, Sands J (1973): Quantitative growth and development of the human brain. Arch Dis Child 48:757–767.

Du AT, Jahng GH, Hayasaka S, Kramer JH, Rosen HJ, Gorno-Tempini ML, Rankin KP, Miller BL, Weiner MW, Schuff N (2006): Hypoperfusion in frontotemporal dementia and Alzheimer disease by arterial spin labeling MRI. Neurology 67:1215–1220.

Fox PT, Raichle ME (1986): Focal physiological uncoupling of cerebral blood flow and oxidative metabolism during somatosensory stimulation in human subjects. Proc Natl Acad Sci USA 83:1140–1144.

Fox PT, Raichle ME, Mintun MA, Dence C (1988): Nonoxidative glucose consumption during focal physiologic neural activity. Science 241:462–464.

Friston KJ, Holmes AP, Worsley KJ, Poline J-P, Frith CD, Frackowiak RSJ (1995): Statistical parametric maps in functional imaging: A general linear approach. Hum Brain Mapp 2:189–210.

Fujita K, Maekawa H, Dairoku H, Yamanaka K (2006): Japanese Wechsler Adult Intelligence Scale, 3rd ed. Tokyo: Nihon Bunka Kagakusha.

Giedd JN, Blumenthal J, Jeffries NO, Castellanos FX, Liu H, Zijdenbos A, Paus T, Evans AC, Rapoport JL (1999): Brain development during childhood and adolescence: A longitudinal MRI study. Nat Neurosci 2:861–863.

Gogtay N, Giedd JN, Lusk L, Hayashi KM, Greenstein D, Vaituzis AC, Nugent TF III, Herman DH, Clasen LS, Toga AW, Rapoport JL, Thompson PM (2004): Dynamic mapping of human cortical development during childhood through early adulthood. Proc Natl Acad Sci USA 101:8174–8179.

Good CD, Johnsrude IS, Ashburner J, Henson RNA, Friston KJ, Frackowiak RSJ (2001): A voxel-based morphometric study of ageing in 465 normal adult human brains. Neuroimage 14:21–36.

Guo X, Chen C, Chen K, Jin Z, Peng D, Yao L (2007): Brain development in Chinese children and adolescents: A structural MRI study. Neuroreport 18:875–880.

Gupta SK, Ratnam BV (2009): Cerebral perfusion abnormalities in children with autism and mental retardation: A segmental quantitative SPECT study. Indian Pediatr 46:161–164.

Huttenlocher PR (1979): Synaptic density in human frontal cortex: Developmental changes and effects of aging. Brain Res 163:195–205.

Huttenlocher PR, de Courten C, Garey LJ, Van der Loos H (1982): Synaptogenesis in human visual cortex—Evidence for synapse elimination during normal development. Neurosci Lett 33:247–252.

Huttenlocher PR, Dabholkar AS (1997): Regional differences in synaptogenesis in human cerebral cortex. J Comp Neurol 387:167–178.

Inoue K, Ito H, Goto R, Nakagawa M, Kinomura S, Sato T, Sato K, Fukuda H (2005): Apparent CBF decrease with normal aging due to partial volume effects: MR-based partial volume correction on CBF SPECT. Ann Nucl Med 19:283–290.

Ito H, Kanno I, Fukuda H (2005): Human cerebral circulation: positron emission tomography studies. Ann Nucl Med 19:65–74.

Johnson MH (2001): Functional brain development in humans. Nat Rev Neurosci 2:475–483.

Lancaster JL, Woldorff MG, Parsons LM, Liotti M, Freitas CS, Rainey L, Kochunov PV, Nickerson D, Mikiten SA, Fox PT (2000): Automated Talairach atlas labels for functional brain mapping. Hum Brain Mapp 10:120–131.

Lenroot RK, Gogtay N, Greenstein DK, Wells EM, Wallace GL, Clasen LS, Blumenthal JD, Lerch J, Zijdenbos AP, Evans AC, Thompson PM, Giedd JN (2007): Sexual dimorphism of brain developmental trajectories during childhood and adolescence. Neuroimage 36:1065–1073.

Maldjian JA, Laurienti PJ, Kraft RA, Burdette JH (2003): An automated method for neuroanatomic and cytoarchitectonic atlas-based interrogation of fMRI data sets. Neuroimage 19:1233–1239.

Mata M, Fink DJ, Gainer H, Smith CB, Davidsen L, Savaki H, Schwartz WJ, Sokoloff L (1980): Activity-dependent energy metabolism in rat posterior pituitary primarily reflects sodium pump activity. J Neurochem 34:213–215.

Matsuda H, Ohnishi T, Asada T, Li ZJ, Kanetaka H, Imabayashi E, Tanaka F, Nakano S (2003): Correction for partial-volume effects on brain perfusion SPECT in healthy men. J Nucl Med 44:1243–1252.

Meltzer CC, Leal JP, Mayberg HS, Wagner HN Jr, Frost JJ (1990): Correction of PET data for partial volume effects in human cerebral cortex by MR imaging. J Comput Assist Tomogr 14: 561–570.

Muller-Gartner HW, Links JM, Prince JL, Bryan RN, McVeigh E, Leal JP, Davatzikos C, Frost JJ (1992): Measurement of radiotracer concentration in brain gray matter using positron emission tomography: MRI-based correction for partial volume effects. J Cereb Blood Flow Metab 12:571–583.

Newberg AB, Wang J, Rao H, Swanson RL, Wintering N, Karp JS, Alavi A, Greenberg JH, Detre JA (2005): Concurrent CBF and CMRGlc changes during human brain activation by combined fMRI-PET scanning. Neuroimage 28:500–506.

Oner O, Oner P, Aysev A, Kucuk O, Ibis E (2005): Regional cerebral blood flow in children with ADHD: Changes with age. Brain Dev 27:279–285.

Ostby Y, Tamnes CK, Fjell AM, Westlye LT, Due-Tonnessen P, Walhovd KB (2009): Heterogeneity in subcortical brain development: A structural magnetic resonance imaging study of brain maturation from 8 to 30 years. J Neurosci 29:11772–11782.

Paus T (2005): Mapping brain maturation and cognitive development during adolescence. Trends Cogn Sci 9:60–68.

Petersen ET, Lim T, Golay X (2006a): Model-free arterial spin labeling quantification approach for perfusion MRI. Magn Reson Med 55:219–232.

Petersen ET, Mouridsen K, Golay X, all named co-authors of the QUASAR test-retest, s(2010): The QUASAR reproducibility study, Part II: Results from a multi-center arterial spin labeling test-retest study. Neuroimage 49:104–113.

Petersen ET, Zimine I, Ho YC, Golay X (2006b): Non-invasive measurement of perfusion: A critical review of arterial spin labelling techniques. Br J Radiol 79:688–701.

Rousset OG, Ma Y, Evans AC (1998): Correction for partial volume effects in PET: Principle and validation. J Nucl Med 39:904–911.

Schoning M, Staab M, Walter J, Niemann G (1993): Transcranial color duplex sonography in childhood and adolescence. Age dependence of flow velocities and waveform parameters. Stroke 24:1305–1309.

Strul D, Bendriem B (1999): Robustness of anatomically guided pixel-by-pixel algorithms for partial volume effect correction in positron emission tomography. J Cereb Blood Flow Metab 19: 547–559.

Talairach J, Tournoux P (1988): Co-Planar Stereotaxic Atlas of the Human Brain: Three-Dimensional Approach System: An Approach to Cerebral Imaging. Stuttgart: Georg Thieme Verlag.

Thatcher RW (1992): Cyclic cortical reorganization during early childhood. Brain Cogn 20:24–50.

Videen TO, Perlmutter JS, Mintun MA, Raichle ME (1988): Regional correction of positron emission tomography data for the effects of cerebral atrophy. J Cereb Blood Flow Metab 8:662–670.

Wang J, Licht DJ (2006): Pediatric perfusion MR imaging using arterial spin labeling. Neuroimag Clin North Am 16:149–167.

Webb SJ, Monk CS, Nelson CA (2001): Mechanisms of postnatal neurobiological development: Implications for human development. Dev Neuropsychology 19:147–171.

Williams DS, Detre JA, Leigh JS, Koretsky AP (1992): Magnetic resonance imaging of perfusion using spin inversion of arterial water. Proc Natl Acad Sci USA 89:212–216.

Ye FQ, Berman KF, Ellmore T, Esposito G, van Horn JD, Yang Y, Duyn J, Smith AM, Frank JA, Weinberger DR, McLaughlin AC (2000): H(2)(15)O PET validation of steady-state arterial spin tagging cerebral blood flow measurements in humans. Magn Reson Med 44:450–456.